Applied Physics Letters ARTICLE scitation.org/journal/apl

Generalized optical design of two-spherical-mirror multi-pass cells with dense multi-circle spot patterns

Cite as: Appl. Phys. Lett. **116**, 091103 (2020); doi: 10.1063/1.5145356
Submitted: 17 January 2020 · Accepted: 23 February 2020 ·
Published Online: 4 March 2020

View Online Export Citation CrossMark

Ruyue Cui,[1,2] Lei Dong,[1,2,a)] Hongpeng Wu,[1,2] Weidong Chen,[3] and Frank K. Tittel[4]

AFFILIATIONS

[1]State Key Laboratory of Quantum Optics and Quantum Optics Devices, Institute of Laser Spectroscopy, Shanxi University, Taiyuan 030006, China
[2]Collaborative Innovation Center of Extreme Optics, Shanxi University, Taiyuan 030006, China
[3]Laboratoire de Physicochimie de l'Atmosphère, Université du Littoral Côte d'Opale, Dunkerque 59140, France
[4]Department of Electrical and Computer Engineering, Rice University, 6100 Main Street, Houston, Texas 77005, USA

[a)]Author to whom correspondence should be addressed: donglei@sxu.edu.cn

ABSTRACT

We report a set of practical multi-circle spot patterns produced by two-spherical-mirror multi-pass cells (MPCs). Such a set of intricate spot patterns takes full account of the evolution and deformation of spot shapes caused by aberrations on two spherical mirror surfaces by means of a multi-ray calculation model, thus avoiding spot overlaps and reducing an etalon effect. An eight- and nine-multi-circle spot pattern was demonstrated experimentally in order to verify the validity of the calculated results. Furthermore, a 2*f* spectrum measurement of ambient methane was performed using the eight-multi-circle spot pattern MPC to verify the practicability. An approach to search for multi-circle spot patterns in a two-spherical-mirror MPC is discussed in detail. A set of dense spot patterns results in sensitive, low-cost, compact trace gas sensors based on MPCs, which can be used to implement a large-scale deployment of distributed sensor networks for monitoring pollutants or to realize handheld mobile sensor devices for safety inspection, leakage detection, and medical diagnostics.

Published under license by AIP Publishing. https://doi.org/10.1063/1.5145356

Multi-pass cells (MPCs) are widely used in spectroscopy to measure low concentration components or to observe weak spectra from trace gases.[1–9] An MPC is composed of two or more mirrors with high reflectivity, in which the light is reflected back and forth many times in the same space, thus producing a long optical path. Currently, the most commonly used two-mirror MPC is the Herriott cell based on two spherical concave mirrors due to its simplicity, reliability, and robustness.[10] However, the circular spot patterns of Herriott cells are sparse with low spot fill factors. In order to improve the utilization efficiency of the mirror surfaces, two aspherical mirrors can be used to replace the two spherical mirrors, thus producing a dense spot pattern.[11] Various dense spot patterns based on two aspherical mirrors have been reported, which realized a high fill factor and long effective optical path length compared to a standard Herriott cell.[12–14] However, the fabrication of aspheric surfaces is more complex, which is due to the fact that the surface accuracy of an aspherical mirror is difficult to guarantee with a design requirement of a complicated curvature. Therefore, a pair of spherical mirrors is always expected to be used in these MPCs because of their simple construction, easy fabrication, and low cost.

In 2015, Liu *et al.* reported an MPC of a seven-multi-circle spot pattern based on two 2-in. spherical mirrors.[15] Such an MPC achieves a 26.4-m optical path length and results in highly sensitive CH_4 detection. However, the lack of theoretical guidance limits the ability to develop other multi-circle spot patterns, which may provide other viable MPC configurations. Recently, we developed a theoretical model of dense spot pattern MPCs, in which a pair of spherical mirrors was employed to create a set of exotic spot patterns with a high fill factor. The seven-multi-circle spot pattern was simulated by our theoretical model as shown in Fig. 3(c) of Ref. 16. However, the developed calculation model did not take into account the variation of spot shapes, due to the use of an ideal single ray. In fact, the deformation of spot shapes generated by the spherical mirror aberrations may lead to overlaps between adjacent spots and hence cause an etalon background. A study of the evolution of spot shapes is necessary in order to obtain practical MPCs.

Published under license by AIP Publishing

In this manuscript, we focus on multi-circle spot patterned MPCs. In our calculation model, an ideal single ray was replaced with a geometric ray set as an incident light beam, so that the evolution of the spot shape can be clearly observed via direct tracing of each separate ray forming the incident light beam. Based on this modified calculation model, a set of practical multi-circle patterns without spot overlaps was identified and verified.

The light beam consists of a plurality of separate rays. These rays are in parallel and encircle a center ray as shown in Fig. 1. The circular outline of the cross section of this ray set defines the initial spot shape of the incident light beam. Each ray in this ray set is independently tracked in a three-dimensional coordinate system using the single ray calculation model[16] as described by the following equation:

$$\begin{bmatrix} A & B \\ C & D \end{bmatrix} = \begin{bmatrix} 1 & 0 \\ L & 1 \end{bmatrix} \cdot \begin{bmatrix} 1 & d_n S \\ 0 & 1 \end{bmatrix}. \tag{1}$$

The ABCD matrix consists of a modified transmission matrix and a modified reflection matrix in which L and S represent two operators. The operators are defined as $L\varphi = -2\arcsin(\varphi/R)$ and $S\varphi = \sin\varphi$, respectively, where R is the curvature radius of the spherical mirrors and is an arbitrary rational number. The parameter d_n is the optical path length for the nth transmission between the two spherical mirrors. The obtained outlines of this ray beam incident on two spherical mirror surfaces were recorded. The spherical mirror aberrations change an initial circular spot into a crescent spot due to its spherical nature as shown in Fig. 1. Therefore, the observation of the spot shape evolution is important, which can effectively avoid overlaps between two adjacent spots on each mirror. Using the multi-ray calculation model, the influence from spherical aberration, astigmatism, and coma can be considered.

In order to identify practical multi-circle spot patterns, a large number of numerical calculations were carried out using Eq. (1). Two 2-in. diameter spherical mirrors were selected with focal lengths of 50 mm. The beam diameter was selected to be 1.0 mm, which is an easily obtained value for a near infrared laser beam. The diameters of both entrance and exit holes were set to be 2 mm. The inclination angle of the incident beam is fixed to $(-7.4°, 3.4°)$, since such an inclination angle was found to decrease the spot divergence. Due to spot overlap, not all multi-circle spot patterns can be adopted in practice. Hence, three criteria are followed: (1) circles do not intersect; (2) spots are evenly distributed on two mirror surfaces; (3) spots do not overlap and the spot size is <2 mm before νth reflections, where ν is as large as possible. With the above fixed parameters, the production of a multi-circle spot pattern strongly depends also on other parameters, such as the initial entry location (x_0, y_0), the mirrors spacing D, and the pass count ν. The process of searching for a practical spot pattern is as follows: the mirror spacing is increased from small to large until a multi-circle spot pattern appears. The initial entry location (x_0, y_0) is adjusted to make the spot pattern zoom in and out around the center point of the mirrors, so that the spots can be evenly distributed on two mirror surfaces and an appropriate pass count ν is determined according to the condition of the overlap of the spots and the size of the exit hole.

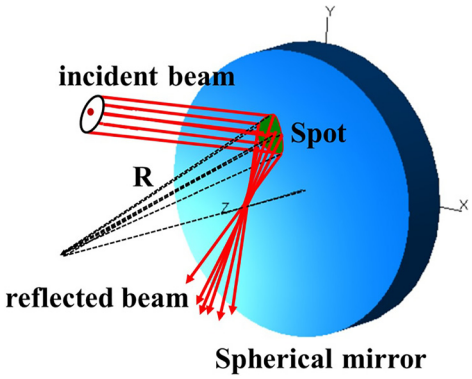

FIG. 1. Reflection of the incident ray set on a spherical mirror.

Practical three-, four-, five-, seven-, eight-, and nine- multi-circle spot patterns are shown in Fig. 2. All spot patterns were projected onto the x-y plane of the exit mirror, respectively. All corresponding parameters for multi-circle spot patterns are listed in Table I. The absence of a six-multi-circle spot pattern is due to the fact that a set of appropriate parameters was not found to evenly distribute the spots of the six-multi-circle pattern on the mirror surface.

When the evolution of the spot shapes is not considered and the incident beam is an ideal ray, the incident ray is able to continue to retrace the same spot pattern.[16] However, the deformation of spot

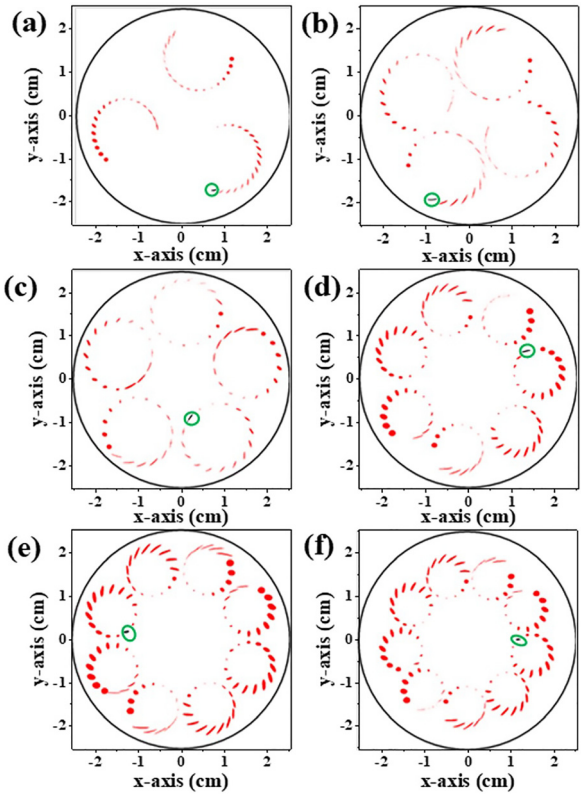

FIG. 2. Six exotic spot patterns generated by a two-spherical-mirror MPC. (a) Three-, (b) four-, (c) five-, (d) seven-, (e) eight-, and (f) nine-multi-circle spot patterns. The plots represent the spot projection of the exit mirror; black spots surrounded by green circles represent the exit positions of the beam.

Published under license by AIP Publishing

TABLE I. Initial entry location (x_0, y_0) on entry mirror, mirror spacing (D), and pass count (ν) used to obtain the pot patterns depicted in Fig. 2; total optical path length (L), volume of MPC (V), and ratio of L to V (RLV); spot location (x_ν, y_ν) on the exit mirror and ray inclination angle (x'_ν, y'_ν) after νth pass count.

Pattern	(x_0, y_0) (mm)	D (mm)	ν	L (m)	V (mL)	RLV (cm^{-2})	(x_ν, y_ν) (mm)	(x'_ν, y'_ν) (°)
Figure 2(a)	(17.58, 10.51)	50.60	107	5.41	102.56	5.27	(7.43, −17.22)	(6.79, 2.87)
Figure 2(b)	(17.38, 11.23)	29.54	133	3.93	59.87	6.56	(−8.66, −19.47)	(1.09, −14.16)
Figure 2(c)	(17.81, 11.46)	69.91	159	11.12	141.70	7.85	(1.79, −9.12)	(14.95, 6.30)
Figure 2(d)	(16.23, 6.94)	123.06	203	24.98	249.42	10.02	(13.36, 6.33)	(8.99, 12.35)
Figure 2(e)	(16.30, 5.83)	138.99	235	32.66	281.71	11.59	(−12.53, 1.79)	(−11.15, −6.32)
Figure 2(f)	(14.91, 6.72)	118.16	223	26.35	239.49	11.00	(11.80, 0.26)	(9.79, 8.80)

shapes resulting from the spherical mirror aberration can cause the spots to overlap before a complete cycle, in which the beam diameter plays an important role. With the 1-mm beam diameter, the five-, eight-, and nine-multi-circle spot patterns in Figs. 2(c), 2(e), and 2(f) can complete a cycle without a spot overlap. The reason why the last few spots were removed in Figs. 2(e) and 2(f) is because their spot sizes exceed 2 mm. These large size spots cannot exit from a 2-mm exit hole. The effective pass counts ν is listed in Table I. In contrast, the spot overlap occurs in the case of a 1-mm beam for the three-, four-, and seven-circle spot patterns after the νth effective pass counts. These overlap spots were removed from Figs. 2(a), 2(b), and 2(d). However, when the beam diameters decrease to 0.6 mm for Fig. 2(a), 0.7 mm for Fig. 2(b), and 0.8 mm for Fig. 2(d), these multi-circle spot patterns are able to be closed.

The initial entry location (x_0, y_0) of the beam can control the spot distribution on the two mirror surfaces. Based on Table I, the values of the initial entry location do not change much for the different spot patterns and are distributed in an annular area with a diameter of 6.4 mm. In order to assess the space utilization of the different spot patterns, a ratio of the total optical path length to the volume, RLV was used as shown in column 7 in Table I. As the number of circles increases, the RLV increases monotonically except for the eight-multi-circle spot pattern. In fact, the total optical path length L equals to the product of the effective pass counts ν and the mirror spacing D, while the volume V equals to the product of the mirror area and the mirror spacing D. Since the mirror area is a constant in our case, the RLV depends on the effective pass counts ν, which means that a higher effective pass count offers a larger RLV. Therefore, the eight-multi-circle spot pattern achieves the largest RLV in the six spot patterns of Table I. In order to verify the validity of the calculation in Fig. 2, the eight- and nine-multi-circle spot patterns in Figs. 2(e) and 2(f) were demonstrated experimentally as shown in Figs. 3(a) and 3(b), respectively. Two 2-in. spherical mirrors with a curvature radius of 100 mm were employed and the mirror reflectivity was 98%. A visible diode laser emitting at 635 nm was used to observe the spot location, shape, and pattern on each mirror. The excellent agreement between the calculation and the experiment confirms the validity of the model. In order to verify the performance of these dense patterned MPCs, the MPC with an eight-multi-circle spot pattern was employed to detect ambient methane (∼1.8 ppm) using a 1.65 μm distributed-feedback laser. Based on the acquired 2f spectrum in Fig. 4, a signal-to-noise ratio of ∼93 was obtained.

Solutions for multi-circle spot patterns not only occur in MPCs consisting of two 2-in. spherical mirrors with a 50-mm focal length, but also are widely present in spherical mirror MPCs. The evolution of the spot pattern in a spherical mirror MPC follows a certain law. To search for the exotic multi-circle spot pattern, the steps necessary are as follows. A small mirror spacing D which is $<R$ should be selected as the initial point. With an increase in D, the chaotic spot patterns evolve into a nested-circle spot pattern as shown in Fig. 5(a). Subsequently, a spot pattern rotating inward appears as shown in Fig. 5(b). When finding this pattern, a small increasing step for D should be used since this pattern rotating inward is close to a target multi-circle spot pattern as shown in Fig. 5(c). It is possible that an

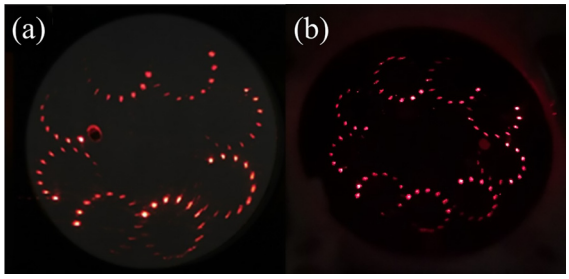

FIG. 3. Photographs of the real (a) eight- and (b) nine-multi circle spot patterns on the exit spherical mirror surfaces.

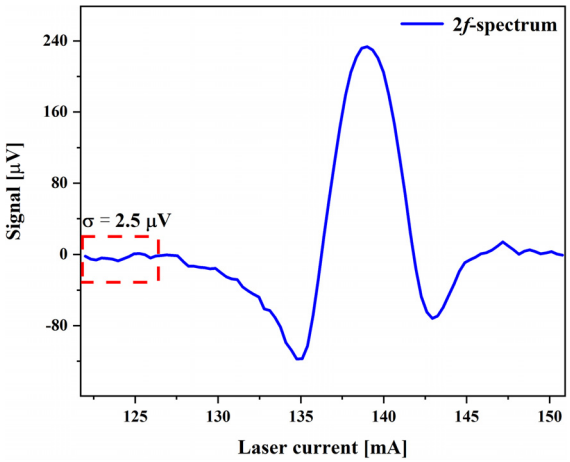

FIG. 4. Ambient CH_4 2f absorption spectrum at a normal atmospheric pressure.

Published under license by AIP Publishing

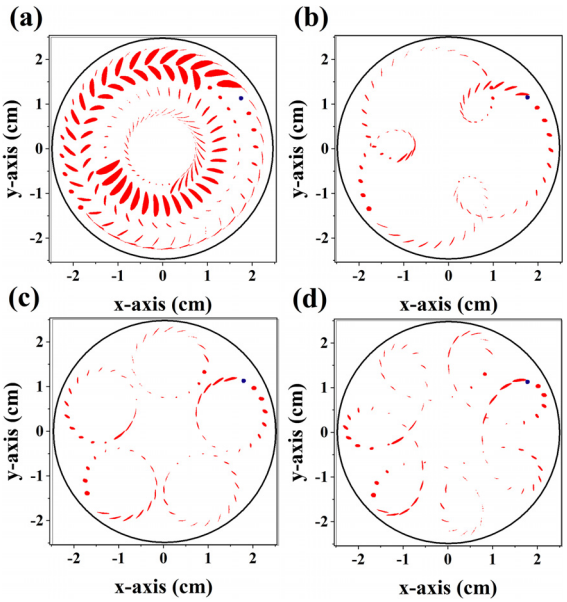

FIG. 5. Evolutionary process of spot patterns on a two-spherical-mirror MPC. (a) Nested-circle spot pattern, (b) spot pattern rotating inward, (c) multi-circle spot pattern, and (d) spot pattern rotating outward.

intersecting-circle spot pattern is obtained unlike several independent circles in Fig. 5(c). In this case, the initial entry location of the incident beam must be adjusted. Not all multi-circle spot patterns can meet the three above-mentioned criteria after trying to adjust all the parameters. With a further increase in D, the spot pattern evolves from the multi-circle spot pattern to a spot pattern rotating outward as shown in Fig. 5(d). Subsequently, the evolution of the spot patterns starts a new circulation and an alternation as in Figs. 5(a)–5(d). Three-, five-, seven-, nine-, eleven-, and thirteen-circle spot patterns appear in turn. When D equals to R, the spherical MPC becomes unstable. After this, thirteen-, eleven-, nine-, seven-, five-, and three-circle spot patterns appear in turn with an increase in D. An obvious regularity of even-circle spot patterns was not found. These even-circle spot patterns occasionally appear between odd-circle spot patterns.

In conclusion, we modified the single ray calculation model for two spherical mirror MPCs into a multi-ray calculation model in which the evolution of the MPC spot shapes on the spherical mirror can be accurately simulated. A set of practical multi-circle spot patterns were identified. These exotic multi-circle spot patterns can offer small sized MPCs with a high fill factor and long absorption length, thus paving the way toward a sensitive, low-cost, compact trace gas sensor suitable for the large-scale deployment of distributed sensor networks and for handheld mobile devices.

This work was supported by the National Key R&D Program of China (No. 2017YFA0304203), National Natural Science Foundation of China (NSFC) (Nos. 61622503, 61575113, 61805132, and 11434007), 111 project (D18001), Outstanding Innovative Teams of Higher Learning Institutions of Shanxi, Foundation for Selected Young Scientists Studying Abroad, Sanjin Scholar (No. 2017QNSJXZ-04), and Shanxi "1331KSC." Frank K. Tittel acknowledges the support from the Robert Welch Foundation (Grant No. #C0586).

REFERENCES

[1] L. Dong, C. Li, N. P. Sanchez, A. K. Gluszek, R. J. Griffin, and F. K. Tittel, Appl. Phys. Lett. **108**, 011106 (2016).
[2] Y. C. Cao, N. P. Sanchez, W. Z. Jiang, R. J. Griffin, F. Xie, L. C. Hughes, C. Zah, and F. K. Tittel, Opt. Express **23**, 2121 (2015).
[3] C. Li, L. Dong, C. Zheng, and F. K. Tittel, Sens. Actuators, B **232**, 188–194 (2016).
[4] W. Ren, L. Q. Luo, and F. K. Tittel, Sens. Actuators, B **221**, 1062 (2015).
[5] L. Dong, F. K. Tittel, C. Li, N. P. Sanchez, H. Wu, C. Zheng, Y. Yu, A. Sampaolo, and R. J. Griffin, Opt. Express **24**, A528–A535 (2016).
[6] L. Dong, Y. Yu, C. Li, S. So, and F. K. Tittel, Opt. Express **23**, 19821–19830 (2015).
[7] R. Cui, L. Dong, H. Wu, S. Li, L. Zhang, W. Ma, W. Yin, L. Xiao, S. Jia, and F. K. Tittel, Opt. Express **26**, 24318 (2018).
[8] J. M. Dang, H. Y. Yu, Y. J. Sun, and Y. D. Wang, Infrared Phys. Technol. **82**, 183 (2017).
[9] R. Ghorbani and F. M. Schmidt, Opt. Express **25**, 12743–12752 (2017).
[10] D. Herriott, H. Kogelnik, and R. Kompfner, Appl. Opt. **3**, 523 (1964).
[11] D. R. Herriott and H. J. Schulte, Appl. Opt. **4**, 883 (1965).
[12] J. A. Silver, Appl. Opt. **44**(31), 6545–6556 (2005).
[13] L. Hao, S. Qiang, G. Wu, L. Qi, D. Feng, Q. Zhu, and Z. Hong, Rev. Sci. Instrum. **73**, 2079 (2002).
[14] S. Ozharar and A. Sennaroglu, Opt. Lett. **42**, 1935 (2017).
[15] K. Liu, L. Wang, T. Tan, G. S. Wang, W. J. Zhang, W. D. Chen, and X. M. Gao, Sens. Actuators, B **220**, 1000 (2015).
[16] R. Cui, L. Dong, H. Wu, S. Li, X. Yin, L. Zhang, W. Ma, W. Yin, and F. K. Tittel, Opt. Lett. **44**(5), 1108 (2019).

Published under license by AIP Publishing